European Congress on Computational Methods
in Applied Sciences and Engineering (ECCOMAS 2012)
J. Eberhardsteiner et.al. (eds.)
Vienna, Austria, September 10-14, 2012

WEAKLY ENFORCED BOUNDARY CONDITIONS FOR THE NURBS-BASED FINITE CELL METHOD

M. Ruess[1], Y. Bazilevs[2], D. Schillinger[3], N. Zander[1], E. Rank[1]

[1]Chair for Computation in Engineering
Technische Universitt Mnchen
Arcisstrasse 21, 80333 Mnchen, Germany
e-mail: {ruess,zander,rank}@bv.tu-muenchen.de

[2] Department of Structural Engineering
University of California San Diego
9500 Gilman Drive, La Jolla, CA 92093, USA
e-mail: jbazilevs@ucsd.edu

[3] Institute for Computational Engineering and Sciences
University of Texas at Austin
201 East 24th Street, Austin, TX 78712
e-mail: dominik@ices.utexas.edu

Keywords: finite cell method, fictitious domain, NURBS, weakly enforced boundary conditions

Abstract. *In this paper, we present a variationally consistent formulation for the weak enforcement of essential boundary conditions as an extension to the finite cell method, a fictitious domain method of higher order. The absence of boundary fitted elements in fictitious domain or immersed boundary methods significantly restricts a strong enforcement of essential boundary conditions to models where the boundary of the solution domain coincides with the embedding analysis domain. Penalty methods and Lagrange multiplier methods are adequate means to overcome this limitation but often suffer from various drawbacks with severe consequences for a stable and accurate solution of the governing system of equations. In this contribution, we follow the idea of* NITSCHE *[29] who developed a stable scheme for the solution of the Laplace problem taking weak boundary conditions into account. An extension to problems from linear elasticity shows an appropriate behavior with regard to numerical stability, accuracy and an adequate convergence behavior. NURBS are chosen as a high-order approximation basis to benefit from their smoothness and flexibility in the process of uniform model refinement.*

1 INTRODUCTION

In contrast to standard finite elements, fictitious domain methods do not require a boundary-fitted mesh. Instead, they embed structures of arbitrarily complex geometry in an analysis domain of simple shape, thus omitting a time-consuming and often not foolproof mesh generation. The finite cell method (FCM) [37, 30] is a high-order approximation scheme that follows the fictitious domain idea. The principle concept of the method is independent of the applied approximation basis and has so far been successfully implemented and investigated for integrated Legendre polynomials [15, 34] as well as for B-spline [37, 35] and NURBS-bases [33]. Like other embedded domain [25, 27] and immersed boundary methods [26, 31] the finite cell method does not require an explicit domain representation in terms of boundary segments or elements but instead exploits recursive bisection [28] to adaptively regain control over the solution domain. However, due to the absence of boundary-fitted elements, the imposition of essential boundary conditions turns out to be a key challenge, which in many cases can largely influence the accuracy of the analysis. A reliable and accurate strong imposition is uncomplicated only in cases where the boundary of the analysis domain fully coincides with the boundary of the solution domain.

Following the weak formulation of the finite element method, several efforts have been made over the years to satisfy essential boundary conditions in a weak sense as an alternative to equivalent pointwise constraints. When weak enforcement of boundary conditions is employed, no explicit constraints on the displacement field are introduced. Instead, the variational formulation of structural mechanics is modified to enforce displacement boundary conditions as Euler–Lagrange conditions. The most popular strategies include the straightforward but variationally not consistent penalty method [3, 40] and the Lagrange Multiplier Method [2, 22, 10, 18] which, though being variationally consistent, introduces additional unknowns and destroys positive definiteness of the augmented system of equations.

Previous work on weak enforcement of essential boundary conditions also includes the pioneering effort of NITSCHE [29] for the Poisson problem that has been successfully adapted in various fields of numerical simulation, such as structural mechanics [19, 17, 21, 16], bone mechanics [34] or fluid mechanics [9, 8]. In this paper, we reconsider this strategy and show that weakly enforced boundary conditions can considerably enhance the flexibility of the finite cell method, since it enables to approximate the physical behavior of arbitrarily constraint problems independently of the geometry and discretization of its embedding domain. A B-spline approximation basis as recently introduced in the FCM [36, 37] is favored in this contribution to exploit the underlying smoothness of B-splines that lead to an increased per-degree-of-freedom accuracy in many FCM computations. This observation is consistent with numerous results of isogeometric structural [12, 13], fluid [1], and fluid-structure interaction [7, 6] analyses, which also employ higher-order continuous basis functions. However, in contrast to the FCM, in isogeometric analysis the complex geometry of interest is always represented with a boundary-fitted mesh.

The paper is outlined as follows. In Section 2, we provide a basic formulation of the FCM including the formulation of the weak boundary conditions applying the B-Spline discretization. In Section 3, we demonstrate with two numerical examples the performance of the proposed methodology. Section 4 summarizes the main findings and draws conclusions.

2 BASIC FORMULATION

The method is formulated for solids of linear elasticity on the basis of the principle of virtual work, independent of the applied Ansatz space. A detailled description of the method particularly with specialization to Legendre-based Ansatz spaces [4, 38] and NURBS [32] can be found e.g. in [37, 34] and [33], respectively.

2.1 The finite cell approach

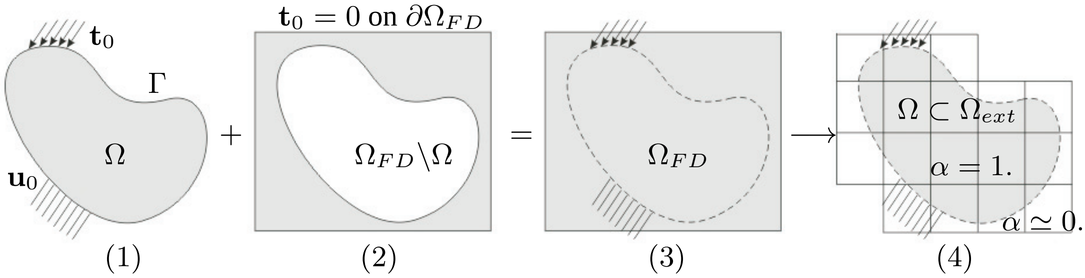

Figure 1: (1) Physical domain Ω with prescribed traction $\mathbf{t}_0$ along the Neumann boundary Γ_N and prescribed displacements $\mathbf{u}_0$ along the Dirichlet boundary Γ_D, (2) extended cell domain $\Omega_{FD} \backslash \Omega$ with zero traction $\mathbf{t}_0$ on the cell domain surface $\partial\Omega_{FD}$, (3) embedded domain with implicit domain support for Ω_{FD} from prescribed displacement constraints on Γ_D and (4) finally applied cell grid structure on Ω_{ext} with location function $\alpha(\mathbf{x})$.

Embedding the physical domain of interest Ω in a fictitious domain Ω_{FD} of much simpler shape (cf. Fig 1(4)), the finite cell method satisfies the weak formulation of the elasticity problem according to the principle of virtual work. The governing integral equations of the formulation are evaluated on Ω only by a refined numerical integration scheme that captures the true boundary Γ (Fig. 1). For a reduced modelling effort the fictitious domain Ω_{FD} is often chosen on a cartesian grid thus taking advantage of the simple rectangular shape and an undistorted mapping to the normalized standard element. The fictitious domain approach is not necessarily restricted to the Cartesian grid and is also applicable for more general extension domains including distorted geometries [34, 30].

The boundary of the extension domain $\Omega_{ext} \subset \Omega_{FD}$ is assumed traction free. Traction forces $\mathbf{t}(\mathbf{x}) = \mathbf{t}_0$ are directly applied on the boundary Γ_t of the true physical domain. In analogy with the Neumann boundary Γ_t, prescribed displacements $\mathbf{u}_0$ are defined along the Dirichlet boundary Γ_u

$$\mathbf{u}(\mathbf{x}) = \mathbf{u}_0 \qquad \forall \mathbf{x} \in \Gamma_u \tag{1}$$

$$\text{where} \qquad \Gamma = \Gamma_u \cup \Gamma_t \quad \wedge \quad \Gamma_u \cap \Gamma_t = \emptyset \tag{2}$$

with $\mathbf{u}$ denoting the displacement vector on Ω_{ext}.

The stress distribution within the embedding domain Ω_{ext} is chosen to be dependent of a location/penalization factor α. For the relation between stresses and strains follows for linear elasticity

$$\boldsymbol{\sigma}_\alpha(\mathbf{x}) = \mathbf{C}_\alpha(\mathbf{x}) : \boldsymbol{\epsilon}(\mathbf{x}) \tag{3}$$

with $\boldsymbol{\epsilon}(\mathbf{x})$ denoting the linear strain tensor and $\mathbf{C}_\alpha(\mathbf{x})$ the elasticity tensor defined as

$$\mathbf{C}_\alpha(\mathbf{x}) \;\; := \;\; \alpha\,\mathbf{C} \quad \begin{cases} \alpha = 1 & \forall\, \mathbf{x} \in \Omega \\ \alpha = \gamma & \forall\, \mathbf{x} \in \Omega_{ext} \setminus \Omega \end{cases} \tag{4}$$

For points inside Ω the elasticity tensor $\mathbf{C}_\alpha$ represents the domain's material properties. For points in Ω_{ext} that are not contained in Ω the factor α penalizes $\mathbf{C}$ by a very small value γ to confine the influence of the extension domain. The choice of γ is a trade-off between accuracy and stability to widely prevent an ill-conditioned system of equations but to ensure convergence. A simple and stable choice can be found e.g. in dependence of the Young's modulus $E(\mathbf{x})$ as $\gamma \approx (E(\mathbf{x}) \cdot \varepsilon^1)$. Volume forces are penalized in analogy to the stresses such that $\mathbf{p}_\alpha(\mathbf{x}) := \alpha\,\mathbf{p}(\mathbf{x})$.

With the relations (3) and (4) and $\Gamma = \{\Gamma_u \cup \Gamma_t\} \subset \Omega_{ext}$ a consistent weak formulation for the linear elasticity problem of Ω on Ω_{ext} is found as

$$\mathcal{W}(u, \delta u) = \mathcal{W}_I(u, \delta u) + \mathcal{W}_E(u, \delta u) \;\; = \;\; 0 \tag{5}$$

with integral terms for the internal and external work, respectively

$$\mathcal{W}_I \;\; = \;\; \int_{\Omega_{ext}} \delta\boldsymbol{\epsilon} : \boldsymbol{\sigma}_\alpha \, dv \tag{6}$$

$$\mathcal{W}_E \;\; = \;\; \int_{\Omega_{ext}} \delta\mathbf{u}^T \mathbf{p}_\alpha \, dv + \int_{\Gamma_t} \delta\mathbf{u}^T \mathbf{t}_0 \, da \tag{7}$$

$$\mathbf{x} \in \Gamma_u \quad \Rightarrow \; \mathbf{u} = \mathbf{u}_0 \tag{8}$$

where $\delta\boldsymbol{\epsilon}$ denotes the variation of the stain tensor with respect to the virtual displacements $\delta\mathbf{u}$.

The equilibrium (5) is consistently extended to a formulation that enforces the essential boundary conditions in a weak sense. Replacing (8) by a weighted integral term over Γ_u and introducing additional terms (cf e.g. [20, 17]) to ensure variational consistency with (5) and to guarantee coercivity, the extension of the principle of virtual displacements has the following form:

$$\begin{aligned} \mathcal{W}_I \;\; = \;\; & \int_{\Omega_{ext}} \delta\boldsymbol{\epsilon} : \boldsymbol{\sigma}(\alpha) \, dv - \int_{\Gamma_u} \delta(\boldsymbol{\sigma}\,\mathbf{n})^T \mathbf{u} \, da - \int_{\Gamma_u} \delta\mathbf{u}^T (\boldsymbol{\sigma}\,\mathbf{n}) \, da \\ & + \tau_S \int_{\Gamma_u} \delta\mathbf{u}^T \mathbf{u} \, da + \tau_N \int_{\Gamma_u} (\mathbf{n}^T \delta\mathbf{u})(\mathbf{u}^T \mathbf{n}) \, da \end{aligned} \tag{9}$$

$$\begin{aligned} \mathcal{W}_E \;\; = \;\; & \int_{\Omega_{ext}} \delta\mathbf{u}^T \mathbf{p}_\alpha \, dv + \int_{\Gamma_t} \delta\mathbf{u}^T \mathbf{t}_0 \, da + \int_{\Gamma_u} \delta\mathbf{t}^T \mathbf{u}_0 \, da \\ & + \tau_S \int_{\Gamma_u} \delta\mathbf{u}^T \mathbf{u}_0 \, da + \tau_N \int_{\Gamma_u} (\mathbf{n}^T \delta\mathbf{u})(\mathbf{u}_0^T \mathbf{n}) \, da \end{aligned} \tag{10}$$

with $(\delta\boldsymbol{\epsilon} : \boldsymbol{\sigma}(\alpha)) = \sum_i \sum_j \delta\epsilon_{ij}\sigma_{ij}$ and τ_N and τ_S denoting penalty parameter with respect to the shear and normal part of the boundary integrals, respectively.

[1] $\varepsilon :=$ unit roundoff

For isotropic material properties equations (9) and (10) split into terms dependent on the Lamé constants λ and μ:

$$\lambda \;:=\; E \cdot \nu/((1+\nu)(1-2\,\nu)) \tag{11}$$

$$\mu \;:=\; E/(1+\nu) \tag{12}$$

with Young's modulus E and poisson ratio ν. With (11) and (12) the stress tensor follows as

$$\boldsymbol{\sigma} \;=\; \lambda\,\nabla\cdot\mathbf{u}\,\mathbf{I} + 2\,\mu\,\boldsymbol{\epsilon} \qquad \text{with} \tag{13}$$

$$\sigma_{ij} \;=\; \sum_k \lambda u_{k,k} + \sum_i\sum_j \mu\,(u_{i,j}+u_{j,i}) \tag{14}$$

Substitution of (13) into (9) and (10) and separation of the terms with regard to the Lamé constants results in a formulation that allows a proper choice of the penalty values τ_S and τ_N subject to μ and λ.

$$\begin{aligned}\mathcal{W}_I \;=\; & \int_{\Omega_{ext}} \delta\boldsymbol{\epsilon} : \boldsymbol{\sigma}(\alpha)\,dv - \lambda\int_{\partial\Omega_u}\delta(\nabla\cdot\mathbf{u}\mathbf{I}\,\mathbf{n})^T\mathbf{u}\,da - \lambda\int_{\partial\Omega_u}\delta\mathbf{u}^T(\nabla\cdot\mathbf{u}\mathbf{I}\,\mathbf{n})\,da \\ & +\tau_N\int_{\partial\Omega_u}(\mathbf{n}^T\delta\mathbf{u})(\mathbf{u}^T\mathbf{n})\,da - \mu\int_{\partial\Omega_u}\delta(\boldsymbol{\epsilon}\,\mathbf{n})^T\mathbf{u}\,da - \mu\int_{\partial\Omega_u}\delta\mathbf{u}^T(\boldsymbol{\epsilon}\,\mathbf{n})\,da \\ & +\tau_S\int_{\partial\Omega_u}\delta\mathbf{u}^T\mathbf{u}\,da\end{aligned} \tag{15}$$

$$\begin{aligned}\mathcal{W}_E \;=\; & \int_{\Omega_{ext}} \delta\mathbf{u}^T\mathbf{p}_\alpha\,dv + \int_{\partial\Omega_t}\delta\mathbf{u}^T\mathbf{t}_0\,da - \lambda\int_{\partial\Omega_u}\delta(\nabla\cdot\mathbf{u}\mathbf{I}\,\mathbf{n})^T\mathbf{u}_0\,da \\ & +\tau_N\int_{\partial\Omega_u}(\mathbf{n}^T\delta\mathbf{u})(\mathbf{u}_0^T\mathbf{n})\,da + \tau_S\int_{\partial\Omega_u}\delta\mathbf{u}^T\mathbf{u}_0\,da + \mu\int_{\partial\Omega_u}\delta(\boldsymbol{\epsilon}\,\mathbf{n})^T\mathbf{u}_0\,da\end{aligned} \tag{16}$$

The boundary terms in (15) and (16) associated with components normal to the boundary are penalized with τ_N the orthogonal terms are penalized with τ_S. For homogeneous boundary conditions the four additional terms in (16) have no contribution to the weak formulation. With

$$\tau_N \;=\; C_N(p)\frac{\lambda}{h} \tag{17}$$

$$\tau_S \;=\; C_S(p)\frac{\mu}{h} \tag{18}$$

the choice of the stability parameters for various discretizations reduces to the choice of the two constants C_N and C_S that are independent of the mesh size h and solely depend on the polynomial degree of the applied Ansatz space.

2.2 B-spline discretization

The finite cells are implemented as hexahedral elements according to the usual principles of finite elements using a tensor product space [11, 5].

In 1D, n shape functions of a B-spline basis of polynomial degree p are specified in a uniformly subdivided parameter space $\Xi = \{\xi_1, \xi_2, \ldots, \xi_{n+p+1}\}$. The $p+1$ equally spaced knots ξ_i define the knot span elements of a B-spline patch analogous to a subdomain of finite elements. Repeated knots lower the continuity between elements. A multiplicity of $p+1$ for knot

ξ_i ensures the corresponding shape function $N_{i,p}$ to be interpolatory at ξ_i. The basis functions of a patch are interpolatory at the first and last knot ξ_1 and ξ_{n+p+1}, respectively, and are $\mathcal{C}^{p-1}$ continuous across the knot span elements. The corresponding knot span is said to be *open* (cf Fig. 2).

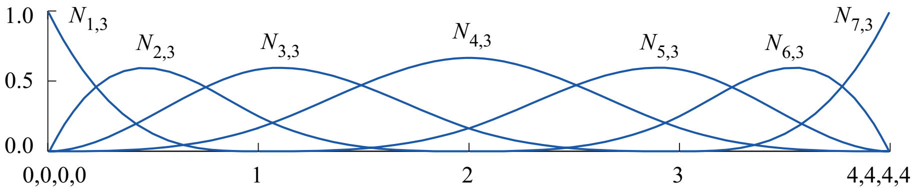

Figure 2: 1D cubic B-spline shape functions $N_{i,3}(i = 1, \ldots, 7)$ across an *open* knot span of four elements. The corresponding parameter space Ξ is specified by a non-decreasing set of knot coordinates ξ_i.

The multivariate B-Spline basis of the finite cells are constructed on the Cartesian product $\Xi \times \mathcal{H} \times \mathcal{Z}$ by the 1D knot spans $\Xi = \{\xi_1, \xi_2, \ldots, \xi_{n+p+1}\}$, $\mathcal{H} = \{\eta_1, \eta_2, \ldots, \eta_{m+p+1}\}$ and $\mathcal{Z} = \{\zeta_1, \zeta_2, \ldots, \zeta_{l+p+1}\}$ [11, 23]. Each shape function is specified by the product

$$Q_{ijk,p}(\xi, \eta, \zeta) \quad = \quad N_{i,p}(\xi)\, M_{j,p}(\eta)\, L_{k,p}(\zeta) \tag{19}$$

with i, j and k indicating the mode position within the product space.

The shape functions (19) are used to specify the Ansatz for the interpolation of the displacement field and corresponding derivatives

$$\mathbf{u} \quad = \quad \mathbf{Q}_p^T(\xi, \eta, \zeta)\, \mathbf{U} \tag{20}$$

with $\mathbf{U}^T = [U_1 \ldots U_N]$ representing the introduced degrees of freedom and $\mathbf{Q}_p$ the interpolation matrix assembled from (19).

The strain tensor $\boldsymbol{\epsilon}$ in (6) is approximated with the linear standard strain operator $\mathbf{B}(\xi, \eta, \zeta)$ that follows from differentiation of the quantities of (20) with respect to the global coordinates $x_i(\xi, \eta, \zeta), (i = 1, 2, 3)$, applying the chain rule [5, 24].

2.3 Numerical integration on cell level

A Gauss-Point integration scheme on sub-cells is applied for the integrals in (15) and (16). This composed integration scheme [39] allows to arbitrarily densify the quadrature points according to the structural needs of the geometric or physical configuration by an independent cell decomposition into smaller units of arbitrary size thus confining the integration error of the implicit domain representation. This approach proved also to produce excellent results for heterogeneous material distributions [34].

For homogeneous material properties, the sub-cell scheme is restricted to boundary cells to capture the true boundary of the physical domain Ω, whereas cells that are completely inside the domain are treated as standard hexahedrals. A tree-based decomposition strategy of the cell domain is favorably applied (Fig. 3) to reduce the integration effort.
With the linear strain operator $\mathbf{B}(\xi, \eta, \zeta)$ and the location dependent material matrix $\mathbf{C}_\alpha$ the cell stiffness is computed as

$$\mathbf{K}_c \quad = \quad \sum_{sc} \left\{ \int_\xi \int_\eta \int_\zeta \hat{\mathbf{B}}^T \mathbf{C}_\alpha \, \hat{\mathbf{B}} \, det(\mathbf{J}_c) \, det(\hat{\mathbf{J}}_{sc}) \, dz_1 \, dz_2 \, dz_3 \right\}$$

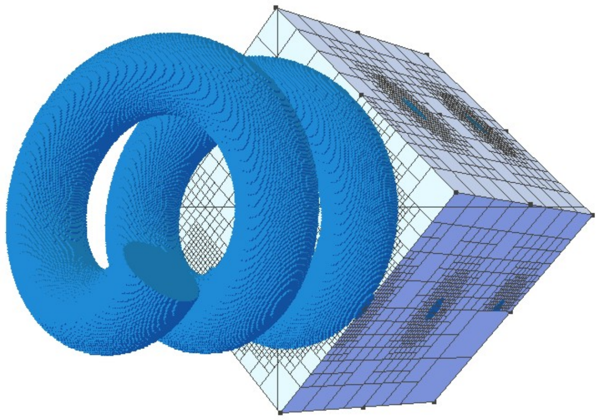

Figure 3: Octree-based cell decomposition into sub-cells for boundary cells of homogeneous material.

with $\mathbf{J}_c$[2] and $\hat{\mathbf{J}}_{sc}$[3] representing the Jacobian of the finite cell and its sub-cells, respectively. The strain interpolation matrix $\hat{\mathbf{B}}$ is evaluated for each sub-cell with regard to the mapping of the sub-cell coordinates of a locally defined Cartesian coordinate system (z_1, z_2, z_3) located in the sub-cell center to the local coordinate system of the finite cell

$$\hat{\mathbf{B}} \quad = \quad \mathbf{B}(\xi(z_1),\, \eta(z_2),\, \zeta(z_3)) \tag{21}$$

The material function $\mathbf{C}_\alpha$ is evaluated at each integration point within the sub-cells. The evaluation of the load integral of (10) follows in analogy to the integration of the stiffness matrix.

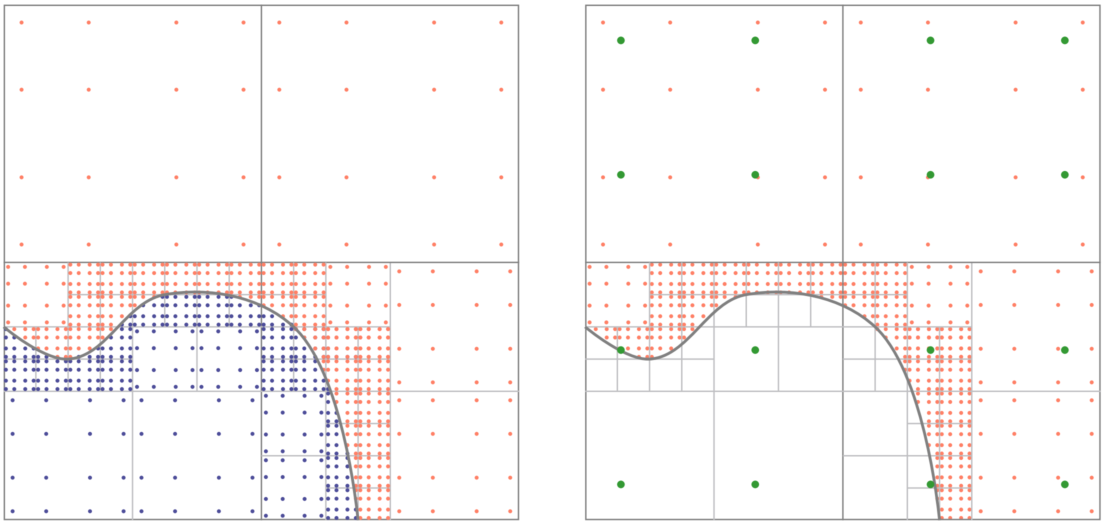

Figure 4: reduced composed integration concept

Figure 4 illustrates an efficient strategy for the composed integration concept that significantly reduces the numerical effort. The left picture of Fig. 4 shows a quadtree-based sub-cell decomposition of a cut boundary cell. Each sub-cell is integrated with $p + 1$ quadrature points.

[2]cell index $\{.\}_c$
[3]sub-cell index $\{.\}_{sc}$

The applied recursive bisection approach densifies the number of sub-cells and thus the number of integration points in the vicinity of the domain boundary Γ. The stresses inside Ω are penalized at each integration point (red points) with $\alpha_\Omega = 1.0$ to account for their full contribution to the governing elasticity equations, resulting in a stiffness contribution $\mathbf{K}_\Omega$. Stresses at the integration points of the extension domain (blue points) are penalized with e.g. $\alpha_{ext} = 10^{-14}$, resulting in a stiffness contribution $\mathbf{K}_{\Omega_{ext}}$, thus fading out any significant contribution from the extension domain Ω_{ext}.

$$\mathbf{K}_c = \mathbf{K}_\Omega(\alpha_\Omega) + \mathbf{K}_{\Omega_{ext}}(\alpha_{ext}) \tag{22}$$

Instead of a numerically demanding sub-cell integration in both domains, Ω and Ω_{ext}, a modified integration concept is followed that reuses the integration result of the true domain to determine the stiffness contribution of the extension domain.

$$\mathbf{K}_c = \mathbf{K}_c(\alpha_{ext}) + \mathbf{K}_\Omega(\alpha_\Omega - \alpha_{ext}) \tag{23}$$

In a first step a penalized stiffness integral for the complete cell domain is computed applying the penalization factor α_{ext}. In a second step, a composed sub-cell integration that is restricted to the the true domain Ω of the cell is performed with $(\alpha_\Omega - \alpha_{ext})$ and added to the cell stiffness.

3 NUMERICAL EXAMPLE

3.1 Plane stress annular plate

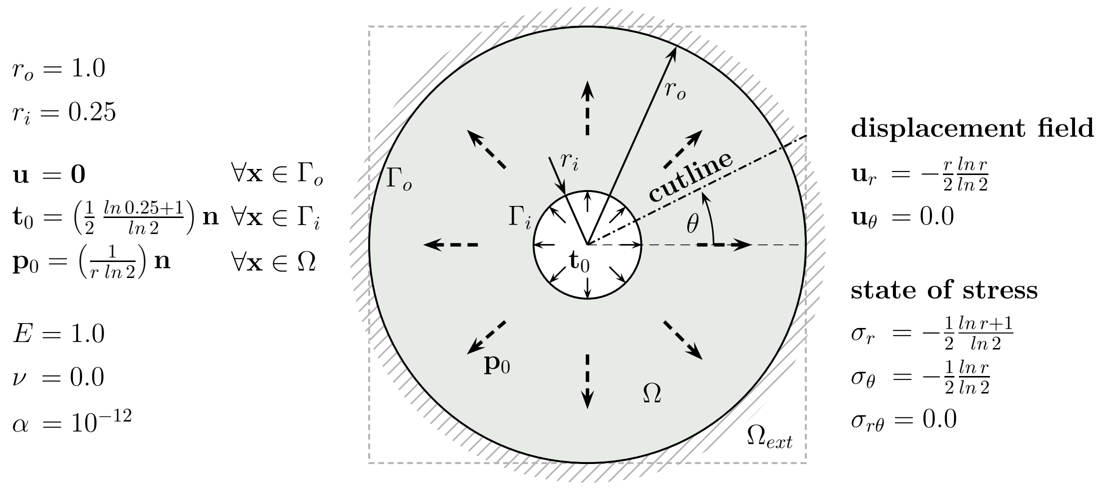

Figure 5: 2D ring plate problem.

A thin plane stress ring plate is modeled to account for the method's performance for problems from linear elasticity. An exact parametric description of the circular boundary was chosen to reduce the modelling error of the problem. Homogeneous Dirichlet boundary conditions are prescribed along the outer radius r_o and a prescribed constant radial pressure force $\mathbf{t}_0$is applied along the inner radius r_i. In addition the plate domain is loaded with a in radial direction exponentially decreasing area load $\mathbf{p}_0$. Geometry, loading, boundary conditions and the analytical reference solution of the displacements field and the state of stress in polar coordinates (r, θ) are provided in Fig. 5. The stability parameter τ_N vanishes with a poisson ratio of $\nu = 0.0$ thus simplifying an optimal choice for the remaining stability parameter τ_S.

Various knot span element discretisations were chosen for a convergence study with uniform p-refinement. We measure the convergence of the analysis in terms of the error in strain energy

$$e_{E(\Omega)} \quad = \quad \left(\frac{|\mathcal{W}(u,u) - \mathcal{W}(\hat{u},\hat{u})|}{|\mathcal{W}(u,u)|} \right)^{\frac{1}{2}} 100\% \tag{24}$$

where u denotes the exact solution, $\hat{u}$ the finite cell solution and $\mathcal{W}(u,u)$ the total strain energy. Figure 6 shows smooth convergence behavior for each model with a slight tendency to exponential rates, resulting in below 1% relative error in energy norm for a (8×8)-knot span element discretization. In contrast to the p-version of the finite cell method [37] that applies high-order quadrilateral cells the B-spline version requires a larger number of knot span elements to ensure the expected convergence behavior.

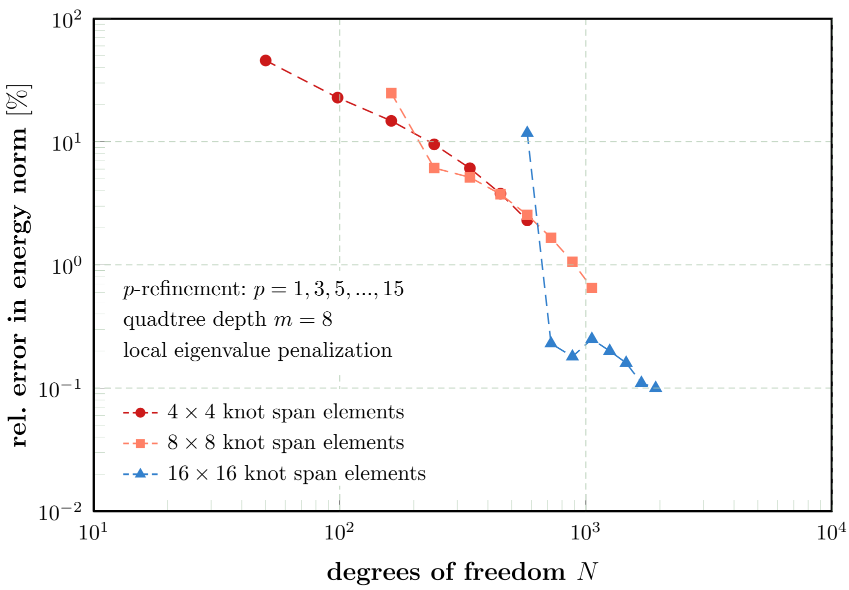

Figure 6: Convergence behavior for uniform p-refinement

Due to the large number of shared spline functions between adjacent knot spans particularly for higher polynomial degrees the numerical effort in terms of degrees of freedom and bandwidth characteristics remains essentially unchanged. The need for a sufficient mesh density is a characteristic of the B-spline version that was found before in [37, 33] for various examples and that can be observed also in Figure 6. The acceptable but moderate convergence progress for (4×4) and (8×8)-knot span elements abruptly jumps down for the (16×16) discretization to an error level that has improved by at least one order of magnitude. The stability parameter for the convergence study were found locally from an eigenvalue analysis [14].

Due to the symmetry of the problem and the symmetric model, a global choice gives reasonable results, too (cf results of Figures 9 and 10). Figure 7-(a) gives an overall impression of the displacement field solution. Even for lower polynomial degrees the depicted smoothness of the displacement field is observed at similar accuracy levels. Figure 7-(b) shows a logarithmic error plot of the absolute error distribution (Vertical dashed lines indicate the interface between Ω and Ω_{ext}). In particular, along the outer radius of the ring plate where homogeneous boundary conditions are weakly enforced a very satisfying result can be noticed without any identifiable

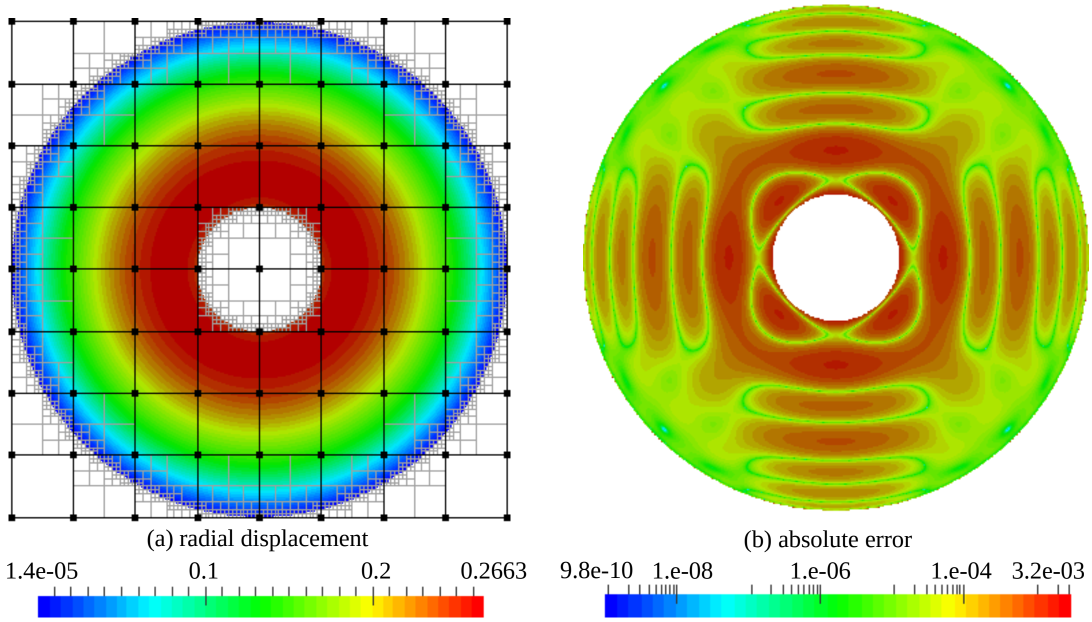

Figure 7: Solution and logarithmic error plot of the displacement field for $p = 8$ and $m = 8$.

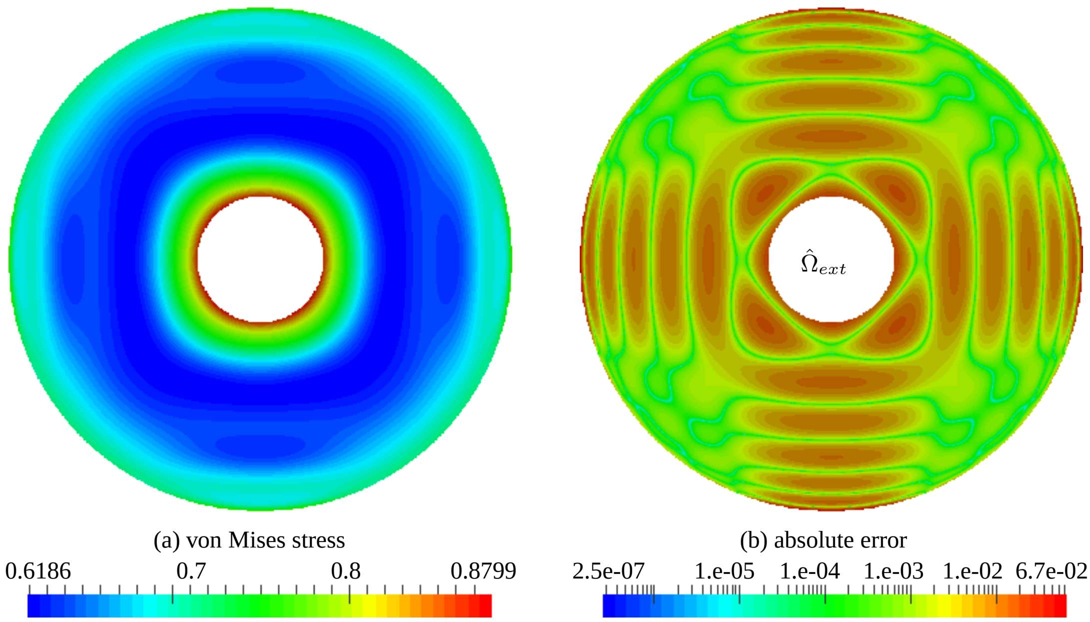

Figure 8: Solution and logarithmic error plot of the von Mises stress distribution for $p = 8$ and $m = 8$.

negative effect from the boundary penalization. The complete symmetry in the error distribution also indicates the high stability of the proposed method.

An equivalent quality of the solution is found for the von Mises stress and corresponding error distribution depicted in Figure 8. The maximum error in the stresses is found along the inner radius. The elements embedding the inner void domain $\hat{\Omega}_{ext}$ $(r < r_i)$ mutually influence a smooth extension of the stresses into $\hat{\Omega}_{ext}$ (cf Fig. 8-(b)) thus introducing a constraint that reflects the maximum error along the inner radius. The very good agreement of the predicted

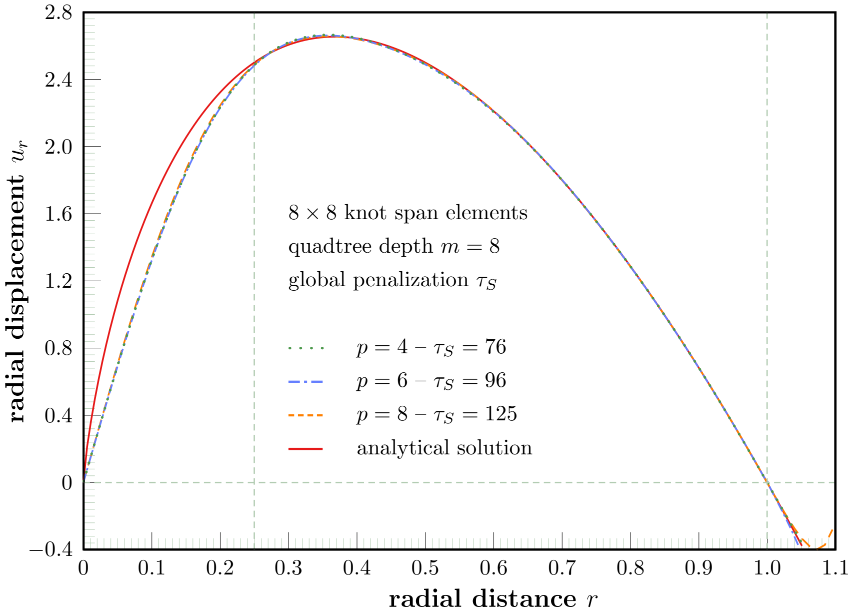

Figure 9: Displacement along a 26 inclined cutline

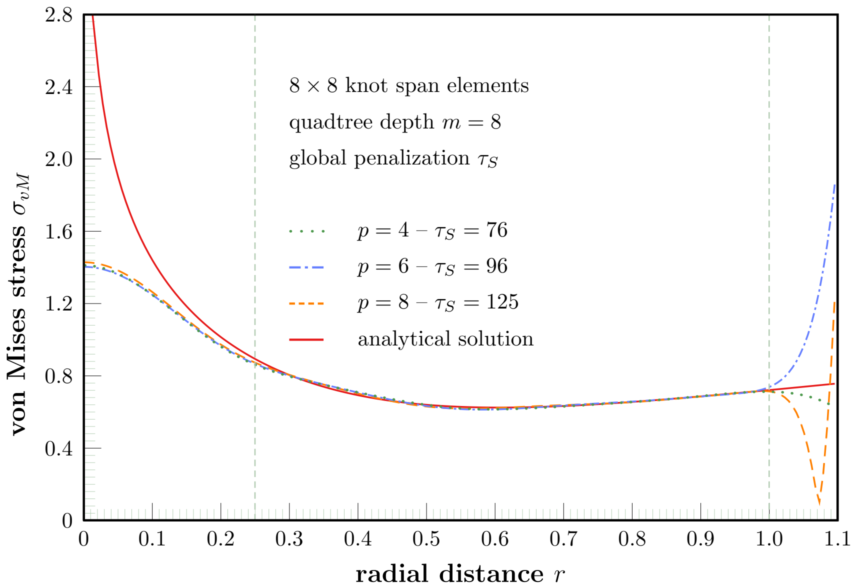

Figure 10: Von Mises stress distribution along a 26 inclined cutline

displacements and stresses with the analytic solution is presented in Figures 9 and 10, respectively. The diagrams show pointwise results along a 26° inclined cutting line from the center to the boundary of the extension domain Ω_{ext} (cf Fig. 5). The displacements are found to be identical within Ω even for the lower polynomial degrees. The von Mises stresses (Fig. 10) show a very accurate agreement with the reference solution, too, with minimal deviations at the inner boundary due to the aforementioned artificial symmetry induced constraints.

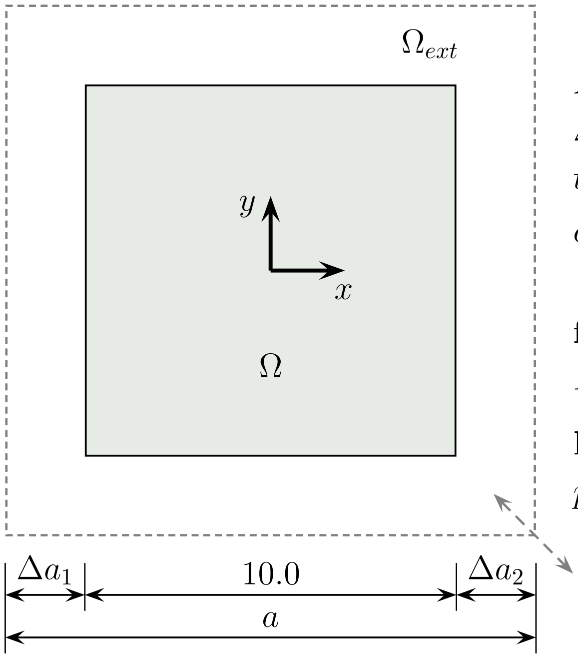

$A_\Omega = 100.0$
$\Delta a_1, \Delta a_2 \geq 0.0$
$t = 0.1$ plate thickness
$\alpha = 10^{-15}$

flexural plate stiffness
$K = \frac{E\,t^3}{12\,(1-\nu^2)}$
loading
$p(x, y) = K/A_\Omega$

Figure 11: Square plate – model parameters.

3.2 Bending of a thin plate

With a second example we demonstrate the performance of the weak boundary formulation for a plate bending problem by comparison with results from a thin plate finite element analysis. The FCM-plate structure is modeled as a 3D solid and eccentrically embedded in a fictitious domain such, that the applied octree depth can not fully resolve the in-plane plate geometry with integration sub-cells. Geometry and material parameters of the model are provided in Figure 11. The plate boundary is fully clamped. An aspect ratio of 100 well-justifies a comparison with a thin plate according to the theory of Kirchhoff-Love [5]. With the chosen load distribution the analytic solution of the Kirchhoff-Love model for the center deflection is independent of the Poisson ratio ν whereas the bending moment strongly depends on ν. In the following a Poisson ratio of $\nu = 0.3$ is chosen to account for the contribution of both stability parameter of the weak boundary formulation, τ_N and τ_S and the corresponding constants C_N and C_S, respectively. Optimal values for C_N and C_S were found experimentally with $C_N = 32$ and $C_S = 32$ resulting in a relative error of the center deflection of below 1% on a 16×16 element grid for both models.

A qualitative comparison of the moment stress resultants $\mathbf{m}_{11}$ and $\mathbf{m}_{12}$ referred to the plate's mid-plane shows virtually no difference in the stress distribution (Fig. 12). A quantitative comparison reveals a relative difference in the extreme values of $0.36\% - 0.48\%$ for $\mathbf{m}_{11}$ and a relative difference of $-2.93 - -3.66\%$ for $\mathbf{m}_{12}$.

4 CONCLUSIONS

With this contribution we introduced an extension to the B-spline version of the finite cell method (FCM) that significantly improves the method's flexibility. The weak imposition of essential boundary conditions based on a conceptional idea proposed by Nitsche [29] for the Poisson problem, represents a variationally consistent formulation of the principle of virtual work. With this extension, the absence of boundary fitted elements in the finite cell method

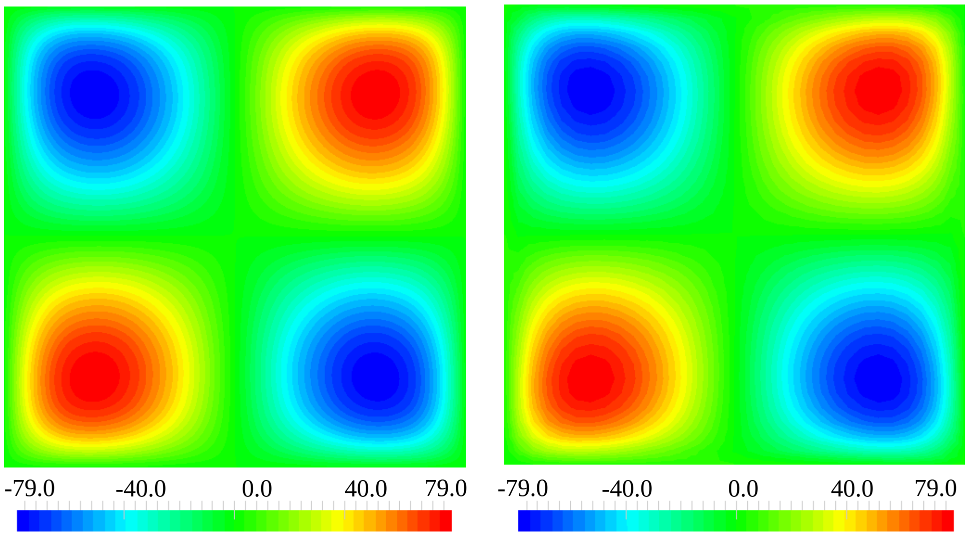

(a) moment stress resultants m_{11} – FCM (left), Kirchhoff-Love (right)

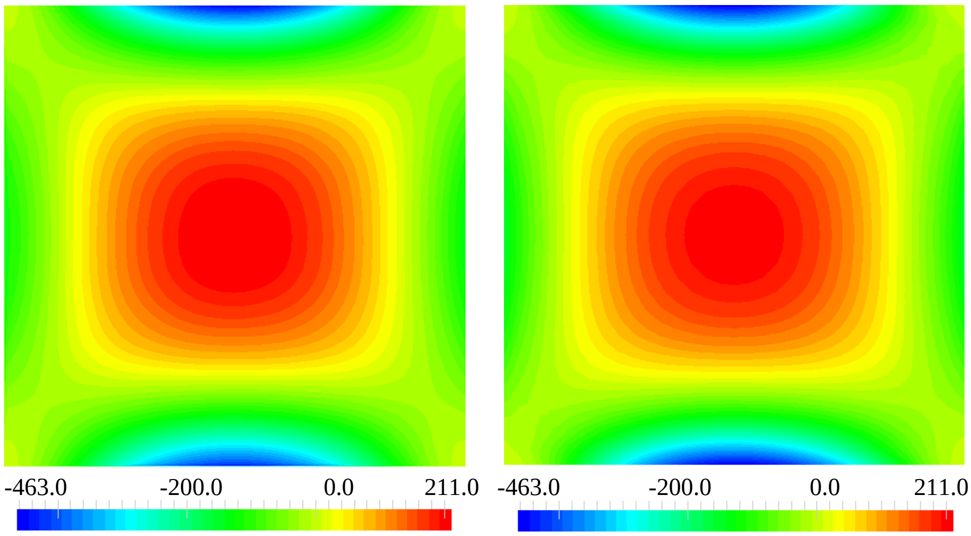

(b) moment stress resultants m_{12} – FCM (left), Kirchhoff-Love (right)

Figure 12: Qualitative comparison of the moment stress resultants referred to the plate's mid-plane for $p = 3$: FCM result with weakly enforced boundary conditions (left) and FEM-Kirchhoff plate result with strong imposed boundary conditions.

is no longer a restriction to domains that coincide with the boundary of the fictitious domain and gives the method more flexibility in the modelling of structures of complex geometry. The method provides reliable results at a reasonably good accuracy level. With a numerical example it was illustrated that convergence can even achieve exponential rates despite the severe challenge of non-matching domain boundaries. A second example demonstrates that the method is competitive with established methods already at moderate polynomial degrees.

REFERENCES

[1] I. Akkerman, Y. Bazilevs, V. M. Calo, T. J. R. Hughes, and S. Hulshoff. The role of continuity in residual-based variational multiscale modeling of turbulence. *Computational Mechanics*, 41:371–378, 2008.

[2] I. Babuška. The Finite Element Method with Lagrangian Multipliers. *Numerische Mathematik*, 20:179–192, 1973.

[3] I. Babuška. The Finite Element Method with penalty. *Mathematics of Computation*, 27(122):221–228, 1973.

[4] I. Babuška, B. A. Szabo, and I. N. Katz. The p-Version of the Finite Element Method. *SIAM Journal on Numerical Analysis*, 18:515–545, 1981.

[5] K.J. Bathe. *Finite element procedures*. Prentice Hall, 1996.

[6] Y. Bazilevs, V. M. Calo, Y. Zhang, and T. J. R. Hughes. Isogeometric fluid-structure interaction analysis with applications to arterial blood flow. *Computational Mechanics*, 38:310–322, 2006.

[7] Y. Bazilevs, M.C. Hsu, J. Kiendl, R. Wüchner, and K.U. Bletzinger. 3d simulation of Wind Turbine Rotors at Full Scale. Part II: Fluid-Structure Interaction. *International Journal for Numerical Methods in Fluids*, 65:236–253, 2011.

[8] Y. Bazilevs, C. Michler, V.M. Calo, and T. J. R. Hughes. Weak dirichlet boundary conditions for wall-bounded turbulent flows. *Computer Methods in Applied Mechanics and Engineering*, 196(49-52):4853–4862, 2007.

[9] Y. Bazilevs, C. Michler, V.M. Calo, and T. J. R. Hughes. Isogeometric variational multiscale modeling of wall-bounded turbulent flows with weakly-enforced boundary conditions on un-stretched meshes. *Computer Methods in Applied Mechanics and Engineering*, 199 (13-16):780–790, 2010.

[10] E. Burman and P. Hansbo. Fictitious domain finite element methods using cut elements: Ii. a stabilized Nitsche method. *Applied Numerical Mathematics*, In Press, Corrected Proof, 2011.

[11] J. A. Cottrell, T. J. R. Hughes, and Y. Bazilevs. *Isogeometric analysis: Towards Integration of CAD and FEM*. John Wiley & Sons, 2009.

[12] J. A. Cottrell, T. J. R. Hughes, and A. Reali. Studies of refinement and continuity in isogeometric structural analysis. *Computer Methods in Applied Mechanics and Engineering*, 196:4160–4183, 2007.

[13] J. A. Cottrell, A. Reali, Y. Bazilevs, and T. J. R. Hughes. Isogeometric analysis of structural vibrations. *Computer Methods in Applied Mechanics and Engineering*, 195:5257–5296, 2006.

[14] J. Dolbow, N. Moës, and T. Belytschko. An extended finite element method for modeling crack growth with frictional contact. *Computer Methods in Applied Mechanics and Engineering*, 190(5152):6825–6846, 2001.

[15] A. Düster, J. Parvizian, Z. Yang, and E. Rank. The finite cell method for three-dimensional problems of solid mechanics. *Computer Methods in Applied Mechanics and Engineering*, 197:3768–3782, 2008.

[16] A. Embar, J. Dolbow, and Isaac Harari. Imposing dirichlet boundary conditions with nitsche's method and spline-based finite elements. *Int. J. Numer. Meth. Engng*, 83(7):877–898, 2010.

[17] S. Fernández-Méndez and A. Huerta. Imposing essential boundary conditions in mesh-free methods. *Computer Methods in Applied Mechanics and Engineering*, 193:1257–1275, 2004.

[18] A. Gerstenberger and W. Wall. An eXtended Finite Element Method / Lagrange Multiplier based approach for fluid-structure interaction. *Computer Methods in Applied Mechanics and Engineering*, 197:1699–1714, 2008.

[19] M. Griebel and M.A. Schweitzer. *A particle-partition of unity method. Part V: Boundary conditions*. Springer-Verlag, Berlin, 2002.

[20] A. Hansbo and P. Hansbo. A finite element method for the simulation of strong and weak discontinuities in solid mechanic. *Comput. Methods Appl. Mech. Engrg*, 193:3523–3540, 2004.

[21] P. Hansbo. Nitsche's method for interface problems in computational mechanics. *GAMM Mitteilungen*, 28/2:183–206, 2005.

[22] P. Hansbo, C. Lovadina, I. Perugia, and G. Sangalli. A lagrange multiplier method for the finite element solution of elliptic interface problems using non-matching meshes. *Numer. Math.*, 100(1):91–115, 2005.

[23] K. Höllig. *Finite Element Methods with B-Splines*. Society for Industrial and Applied Mathematics, Philadelphia, 2003.

[24] T. J. R. Hughes. *The Finite Element Method: Linear Static and Dynamic Finite Element Analysis*. Dover Publications, 2000.

[25] R. Löhner, J.R. Cebral, F.F. Camelli, J.D. Baum, E.L. Mestreau, and O.A. Soto. Adaptive embedded/immersed unstructured grid techniques. *Archives Of Computational Methods In Engineering*, 14:279–301, 2007.

[26] R. Mittal and G. Iaccarino. Immersed Boundary Method. *Annual Review Fluid Mechanics*, 37:239–260, 2005.

[27] P. Neittaanmäki and D. Tiba. An embedding of domains approach in free boundary problems and optimal design. *SIAM Journal on Control and Optimization*, 33(5):1587–1602, 1995.

[28] A. Niggl, E. Rank, R.-P. Mundani, and H.-J. Bungartz. Organizing a p-version finite element computation by an octree-based hierarchy. In P. Díez and N.-E. Wiberg, editors, *Proceedings of the Second International Conference on Adaptive Modeling and Simulation*, pages 26–35, Barcelona, Spain, 2005.

[29] J. Nitsche. Über ein Variationsprinzip zur Lösung von Dirichlet-Problemen bei Verwendung von Teilräumen, die keinen Randbedingungen unterworfen sind. *Abhandlung aus dem Mathematischen Seminar der Universität Hamburg*, 36:9–15, 1970.

[30] J. Parvizian, A. Düster, and E. Rank. Finite cell method – h- and p-extension for embedded domain problems in solid mechanics. *Computational Mechanics*, 41:121–133, 2007.

[31] C. Peskin. The Immersed Boundary Method. *Acta Numerica*, 11:1–39, 2002.

[32] L. Piegl and W. Tiller. *The Nurbs Book*. Springer-Verlag, 2. edition, 1997.

[33] E. Rank, M. Ruess, S. Kollmannsberger, D. Schillinger, and A. Düster. Geometric modeling, Isogeometric Analysis and the Finite Cell Method. *Computer Methods in Applied Mechanics and Engineering*, DOI: 10.1016/j.cma.2012.05.022, 2012.

[34] M. Ruess, D. Tal, N. Trabelsi, Z. Yosibash, and E. Rank. The Finite Cell Method for bone simulations: Verifcation and validation. *Biomechanics and Modeling in Mechanobiology*, 11(3):425–437, 2012.

[35] D. Schillinger, A. Düster, and E. Rank. The hp-d adaptive Finite Cell Method for geometrically nonlinear problems of solid mechanics. *International Journal for Numerical Methods in Engineering*, DOI: 10.1002/nme.3289, 2011.

[36] D. Schillinger and E. Rank. An unfitted hp adaptive finite element method based on hierarchical B-splines for interface problems of complex geometry. *Computer Methods in Applied Mechanics and Engineering*, 200(47-48):3358–3380, 2011.

[37] D. Schillinger, M. Ruess, N. Zander, Y. Bazilevs, A. Düster, and E. Rank. Small and large deformation analysis with the p- and B-spline versions of the Finite Cell Method. *Computational Mechanics*, DOI: 10.1007/s00466-012-0684-z, 2012.

[38] B.A. Szabó, A. Düster, and E. Rank. The p-version of the Finite Element Method. In E. Stein, R. de Borst, and T. J. R. Hughes, editors, *Encyclopedia of Computational Mechanics*, volume 1, chapter 5, pages 119–139. John Wiley & Sons, 2004.

[39] Z. Yang, M. Ruess, S. Kollmannsberger, A. Düster, and E. Rank. An efficient integration technique for the voxel-based Finite Cell Method. *International Journal for Numerical Methods in Engineering*, accepted, 2012.

[40] T. Zhu and S.N. Atluri. A modified collocation method and a penalty formulation for enforcing the essential boundary conditions in the element free galerkin method. *Computational Mechanics*, 21(3):211–222, 1998.